Received: 14 April 2021 | Revised: 7 June 2021 | Accepted: 23 June 2021

DOI: 10.1049/rpg2.12245

IET Renewable Power Generation

The Institution of Engineering and Technology WILEY

ORIGINAL RESEARCH PAPER

Test methodology for validation of multi-frequency models of renewable energy generators using small-signal perturbations

Behnam Nouri[1] | **Łukasz Kocewiak**[2] | **Shahil Shah**[3] | **Przemyslaw Koralewicz**[3] | **Vahan Gevorgian**[3] | **Poul Sørensen**[1]

[1] DTU Wind Energy Department, Technical University of Denmark, Roskilde, Denmark

[2] Power System Solutions, Ørsted A/S, Gentofte, Denmark

[3] Power Systems Engineering Center, National Renewable Energy Laboratory (NREL), Golden, Colorado, USA

Correspondence
Behnam Nouri, DTU Wind Energy Department, Technical University of Denmark, Risø Campus, 4000 Roskilde, Denmark.
Email: beno@dtu.dk

Funding information
European Union's Horizon 2020 Research and Innovation Programme, Grant/Award Number: 691714

Abstract

Providing trustworthy and accurate multi-frequency (or harmonic) models for renewable energy generators (REG) is an ongoing challenge for harmonic studies. There have been effective attempts to propose and design a test device to validate the harmonic models, mainly based on shunt current perturbations. However, using additional devices for perturbations is costly for converter-based test sites. This paper provides the test specifications to extend the application of the grid emulators for voltage perturbations and appropriate harmonic model validation. Besides, the effects of the sequence couplings, initial emissions, and power set-points on the test results have been overlooked in the literature. Considering these effects, this paper proposes a generic test methodology to obtain more accurate models in the sequence domain. The experimental verification of the proposed methodology is demonstrated using a 7 MVA grid emulator for testing of a 2 MVA photo-voltaic converter and a 2 MVA Type 3 wind turbine. This way, the test challenges, specifications, and recommendations are presented using the MW-scale experiments on different REGs. Furthermore, the effects of sequence couplings and initial emissions on the calculation results are investigated and compared. The proposed methodology is applicable for harmonic model validation as well as empirical modelling.

1 | INTRODUCTION

Multi-frequency (or harmonic) interaction is an increasing challenge in converter-dominated power systems, especially in renewable power generation units. To date, several resonance, and harmonic amplification issues have been reported from renewable energy generators (REG), such as wind and photo-voltaic (PV) generations, as well as transmission systems in the literature [1–5].

Consequently, frequency-domain and time-domain studies have been conducted for stability and steady-state analysis of REGs and power systems concerning harmonics [5–11]. In this way, the impedance-based modelling and analysis are introduced and developed for grid-connected power converters to identify and mitigate the potential harmonic issues [6–11]. Furthermore, several international standards and technical recommendations have been issued to harmonise the international academic and industrial efforts on harmonic stability studies and modelling of power systems [12–15].

The trustworthiness and accuracy of the provided models are crucial to achieving correct study results. Ref. [16] introduces a validation approach based on analysing power quality measurements and providing validation margins for each harmonic. In [17–25], impedance measurement test topologies have been proposed using small-signal perturbations via converter-based devices. A perturbation can be either a voltage source in series or a current source parallel with the AC grid [18–23], as illustrated in Figure 1. The perturbation tests are based on the harmonic linearisation concept [17]. Accordingly, it is assumed that the presence of one single frequency (or single-tone) perturbation at the terminal of a device under test (DUT) would excite the same frequency and all related couplings in the DUT response [6, 17–19]. Another option for perturbation is multi-tone, which is a combination of a

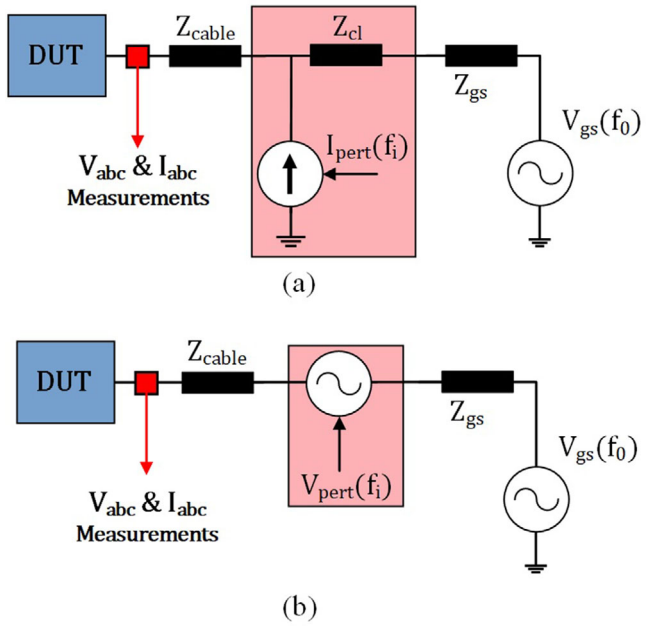

FIGURE 1 Schematic illustration of (a) current and (b) voltage perturbation test topologies in test sites

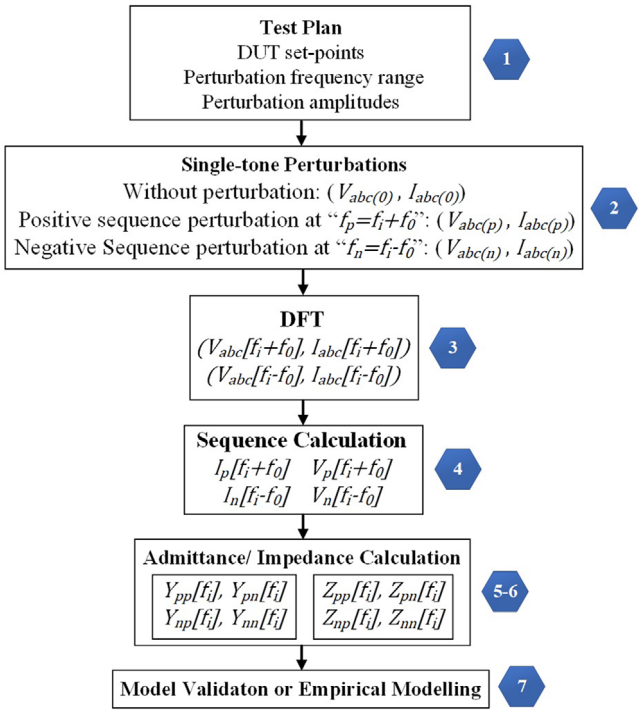

FIGURE 2 Admittance/impedance measurement test methodology for REGs using a test bench

group of single-tone perturbations with limited amplitudes [20]. However, the couplings and interactions among different frequencies in converters would impose additional uncertainties on the results of multi-tone perturbations [7–9, 20].

In [18–24], the experimental implementation of current perturbation ($I_{\text{pert}}(f_h)$) using an additional shunt device is explained and demonstrated, as shown in Figure 1(a). Accordingly, the series-connected impedance (Z_{cl}) is used to divert the perturbation current flow towards the DUT [22]. The design aspects of a test device for the realisation of current perturbations in low voltage (LV), medium voltage (MV), and high voltage (HV) levels are explained in [23]. Besides, series voltage perturbation ($V_{\text{pert}}(f_h)$) is another method for impedance measurement test, as illustrated in Figure 1(b). However, using an additional series-connected device is not an efficient approach since it should be over-designed to withstand the DUT's nominal current [18]. Providing pure single-tone current or voltage perturbations in the MV and HV levels is challenging and costly [18, 20, 23]. In addition, the effects of the sequence couplings, initial emissions, and power set-points have been overlooked in the impedance measurement procedures [18, 20, 21, 23, 24]. The frequency and sequence couplings are most likely for converter-based systems due to the potential nonlinear control systems and three-phase asymmetry, respectively [19, 25].

Nowadays, state-of-the-art test benches are established using back-to-back converters to emulate a flexible and isolated AC grid for grid code compliance testing of REGs [26, 27]. In [8, 29–31], it is attempted to utilise the grid emulator system for voltage perturbations without additional devices. Accordingly, the voltage perturbation concept (Figure 1(b)) can be realised only by adjusting the control system of the grid emulators [29, 30]. However, to the best of our knowledge, there is no specification for a reliable test and validation procedure in the literature. Securing proper test conditions, selecting appropriate amplitude and frequency range for perturbations, and accurate model calculations are essential factors for the trustworthiness of the results.

This paper proposes a practical test methodology along with technical specifications based on small-signal perturbations in the sequence domain. Furthermore, the effects of the sequence couplings and initial emissions on the test results are investigated. The proposed methodology is applicable for multi-frequency model validation and empirical modelling of REGs. In this way, the proposed test methodology is described in Part 2. The potential constraints and technical recommendations for reliable test results are introduced, and solutions are provided in Part 3. The experimental verification of the method using a 7 MVA grid emulator is demonstrated and summarised in Part 4.

2 | PROPOSED TEST METHODOLOGY FOR HARMONIC MODEL VALIDATION AND EMPIRICAL MODELLING

This part illustrates the proposed test methodology for model validation as well as empirical modelling. The flowchart of the proposed test methodology is illustrated in Figure 2. Accordingly, the test methodology is described as follows:

2.1 | Test plan

Schematic diagram of voltage perturbation tests is illustrated in Figure1(a). $V_{\text{pert}}(f_i)$ depicts the voltage perturbation reference at frequency of "f_i". The response of the device under test (DUT) is measured at the point of connection (i.e. V_{abc}, I_{abc}). The first spet towards the impedance measurement tests is to schedule a proper test plan. The test plan includes perturbation amplitude and frequency ranges, power set-points for the DUT. Furthermore, there could be additional set-points for the DUT such as rotor speed, protection scheme, number of involving modules in the test, and switching commands for control systems and breakers. The perturbations can be performed through an automatic test schedule and the set-points would be defined before initiating the tests [29–32].

2.2 | Single-tone perturbations

According to [8] and [19], two different single-tone perturbations are required to determine the DUT model out of the measurement data. Since there could be potential asymmetry and couplings in the DUT control system, it is recommended to perform one perturbation in the positive sequence and the other one in the negative sequence separately. In this way, the measured data from positive sequence test at frequency of "$f_p = f_i + f_0$" ($V_{abc(p)}, I_{abc(p)}$) and negative sequence test at frequency of "$f_n = f_i - f_0$" ($V_{abc(n)}, I_{abc(n)}$) are used for sequence-domain admittance or impedance calculations at frequency of "f_i" [8] and [19]. f_0 stands for the fundamental frequency of the test system. Besides, the normal operation condition without any perturbation ($V_{abc(0)}, I_{abc(0)}$) should be used to eliminate effects of the initial harmonic emissions from DUT or grid emulator on the test results. The initial emissions nay not be important for harmonic stability and resonance studies, but it is necessary for accurate model validation purposes. This fact has been neglected in most of the test and validation procedures in the literature such as [10, 19], and [30]. However, since the harmonic emissions are limited and exist only in a few frequencies, the validation test results would be affected only in a few frequencies. Further investigations are demonstrated in Part 4 of this paper.

2.3 | Discrete Fourier transform

The discrete Fourier transform (DFT) calculation method for assessing the DUT harmonic emissions is provided in IEC 61000-4-7 standard [33]. Accordingly, 0.2 s DFT window (10 cycles in 50 Hz systems and 12 cycles in 60 Hz system) can be used for the harmonic spectrum with 5Hz resolution. However, this paper recommends using 1 s DFT window for precise harmonic stability studies obtaining 1 Hz frequency resolution. Using 1 s DFT window can perform additional averaging on the DUT response and reduce noise effects on the result too. Besides, for perturbation frequencies that are not integer multiples of 5 Hz, it is necessary to have a higher DFT window to calculate the accurate harmonic spectrum for the injected perturbation frequencies. Therefore, this paper applies 1 s DFT window in calculations.

2.4 | Sequence-domain calculation

Admittance or impedance calculations for REGs and converters have been proposed in DQ-frame (or rotating-frame), $\alpha\beta$-frame (or stationary-frame), and sequence-domain in the literature [5–12]. Using sequence-domain models facilitate the harmonic stability studies for networked converters and power systems [6–8]. This is due to the fact that the sequence-domain models are not tied to any local reference frame. Furthermore, different electrical components of a power system have equivalent models in the sequence-domain. Therefore, the sequence-domain models can be easily combined with the rest of a power system for harmonic stability studies [6–8]. Positive and negative sequence models include any potential asymmetry and couplings in the DUT response as well. Therefore, this paper recommends calculation of the sequence-domain models using the DFT values from the previous step as follows:

$$\begin{pmatrix} V_p^i \\ V_n^i \\ V_0^i \end{pmatrix} = \frac{1}{3}\begin{pmatrix} 1 & \alpha & \alpha^2 \\ 1 & \alpha^2 & \alpha \\ 1 & 1 & 1 \end{pmatrix}\begin{pmatrix} V_a^i \\ V_b^i \\ V_c^i \end{pmatrix} \tag{1}$$

Where, $\alpha = 1\angle 120^0$. Note that the zero sequence component (V_0) can be neglected in the case of three-phase three-wire systems. Similar calculations can be used for currents.

2.5 | Norton model calculation

The grid emulator injects voltage perturbations to the terminal of DUT. Consequently, the voltage perturbation (V^i) is considered as input, and the current response (I^i) is reflected as output of the DUT system. Simplified conventional equations have been used for admittance calculations in the literature as follows [8, 10, 19], and [30]:

$$\begin{aligned} Y_{pp}^i &= \frac{I_{p(p)}^{i1}}{V_{p(p)}^{i1}}, \quad Y_{pn}^i = \frac{I_{p(n)}^{i1}}{V_{n(n)}^{i2}} \\ Y_{nn}^i &= \frac{I_{n(n)}^{i2}}{V_{n(n)}^{i2}}, \quad Y_{np}^i = \frac{I_{n(p)}^{i2}}{V_{p(p)}^{i1}} \end{aligned} \tag{2}$$

Where V_p^{i1} and I_p^{i1} are the positive sequence perturbation data at frequency of "$f_i + f_0$", and V_n^{i2} and I_n^{i2} are the negative sequence perturbation data at frequency of "$f_i - f_0$" respectively. Note that the negative sequence component has "$-2f_0$"

frequency shift from the positive sequence, which is called "mirror frequency coupling (MFC)" [7–10, 19]. In addition, Y^i_{pp} and Y^i_{nn} are self admittances at positive and negative sequences, and Y^i_{np} and Y^i_{pn} are coupling admittances between positive and negative sequences at "f_i". However, the effects of the initial emissions and sequence couplings have been neglected in Equation (2). This section provides more accurate equations for the admittance calculations considering the couplings and initial emissions in a test environment. According to IEC 61400-21-3 [14], the multi-frequency model of the DUT at frequency of "f_i" can be regarded as a Norton equivalent as follows:

$$\begin{aligned} I^{i1}_{p} &= Y^i_{pp} V^{i1}_{p} + Y^i_{pn} V^{i2}_{n} + I^{i1}_{p0} \\ I^{i2}_{n} &= Y^i_{np} V^{i1}_{p} + Y^i_{nn} V^{i2}_{n} + I^{i2}_{n0} \end{aligned} \tag{3}$$

Accordingly, using pure single-tone voltage perturbations for positive and negative sequences, measured data can be illustrated for the ith frequency as follows:

$$\begin{pmatrix} V^{i1}_{p(0)} & V^{i2}_{n(0)} & 1 \\ V^{i1}_{p(p)} & V^{i2}_{n(p)} & 1 \\ V^{i1}_{p(n)} & V^{i2}_{n(n)} & 1 \end{pmatrix} \begin{pmatrix} Y^i_{pp} \\ Y^i_{pn} \\ I^i_{p0} \end{pmatrix} = \begin{pmatrix} I^{i1}_{p(0)} \\ I^{i1}_{p(p)} \\ I^{i1}_{p(n)} \end{pmatrix}$$

$$\begin{pmatrix} V^{i1}_{p(0)} & V^{i2}_{n(0)} & 1 \\ V^{i1}_{p(p)} & V^{i2}_{n(p)} & 1 \\ V^{i1}_{p(n)} & V^{i2}_{n(n)} & 1 \end{pmatrix} \begin{pmatrix} Y^i_{np} \\ Y^i_{nn} \\ I^i_{n0} \end{pmatrix} = \begin{pmatrix} I^{i2}_{n(0)} \\ I^{i2}_{n(p)} \\ I^{i2}_{n(n)} \end{pmatrix} \tag{4}$$

Where (0) suffixes indicate the measurement data at a normal operation without any perturbation. Moreover, (*p*) suffixes indicate the data for positive sequence perturbation, and (*n*) suffixes depict the data for negative sequence perturbation for each ith frequency. The Equation (4) can be simplified by subtracting all rows by the normal operation data (0), which leads to:

$$\begin{pmatrix} V^{i1}_{p(p)} - V^{i1}_{p(0)} & V^{i2}_{n(p)} - V^{i2}_{n(0)} \\ V^{i1}_{p(n)} - V^{i1}_{p(0)} & V^{i2}_{n(n)} - V^{i2}_{n(0)} \end{pmatrix} \begin{pmatrix} Y^i_{pp} \\ Y^i_{pn} \end{pmatrix} = \begin{pmatrix} I^{i1}_{p(p)} - I^{i1}_{p(0)} \\ I^{i1}_{p(n)} - I^{i1}_{p(0)} \end{pmatrix}$$

$$\begin{pmatrix} V^{i1}_{p(p)} - V^{i1}_{p(0)} & V^{i2}_{n(p)} - V^{i2}_{n(0)} \\ V^{i1}_{p(n)} - V^{i1}_{p(0)} & V^{i2}_{n(n)} - V^{i2}_{n(0)} \end{pmatrix} \begin{pmatrix} Y^i_{np} \\ Y^i_{nn} \end{pmatrix} = \begin{pmatrix} I^{i2}_{n(p)} - I^{i2}_{n(0)} \\ I^{i2}_{n(n)} - I^{i2}_{n(0)} \end{pmatrix} \tag{5}$$

This way, the effects of the initial harmonic emissions on the calculation results can be eliminated. The emissions in the normal operation could be generated by the DUT or the grid emulator and are neglected in the literature [10, 19], and [30]. Solving Equation (5) leads to admittance calculations as follows:

$$\begin{aligned} Y^i_{pp} &= \frac{\Delta I^{i1}_{p(p)}}{\Delta V^{i1}_{p(p)}} \frac{\left(1 - \frac{\Delta I^{i1}_{p(n)}}{\Delta I^{i1}_{p(p)}} \frac{\Delta V^{i2}_{n(p)}}{\Delta V^{i2}_{n(n)}}\right)}{\left(1 - \frac{\Delta V^{i1}_{p(n)}}{\Delta V^{i1}_{p(p)}} \frac{\Delta V^{i2}_{n(p)}}{\Delta V^{i2}_{n(n)}}\right)} \\ Y^i_{pn} &= \frac{\Delta I^{i1}_{p(n)}}{\Delta V^{i2}_{n(n)}} \frac{\left(1 - \frac{\Delta I^{i1}_{p(p)}}{\Delta I^{i1}_{p(n)}} \frac{\Delta V^{i1}_{p(n)}}{\Delta V^{i1}_{p(p)}}\right)}{\left(1 - \frac{\Delta V^{i1}_{p(n)}}{\Delta V^{i1}_{p(p)}} \frac{\Delta V^{i2}_{n(p)}}{\Delta V^{i2}_{n(n)}}\right)} \\ Y^i_{nn} &= \frac{\Delta I^{i2}_{n(n)}}{\Delta V^{i2}_{n(n)}} \frac{\left(1 - \frac{\Delta I^{i2}_{n(p)}}{\Delta I^{i2}_{n(n)}} \frac{\Delta V^{i1}_{p(n)}}{\Delta V^{i1}_{p(p)}}\right)}{\left(1 - \frac{\Delta V^{i1}_{p(n)}}{\Delta V^{i1}_{p(p)}} \frac{\Delta V^{i2}_{n(p)}}{\Delta V^{i2}_{n(n)}}\right)} \\ Y^i_{np} &= \frac{\Delta I^{i2}_{n(p)}}{\Delta V^{i1}_{p(p)}} \frac{\left(1 - \frac{\Delta I^{i2}_{n(n)}}{\Delta I^{i2}_{n(p)}} \frac{\Delta V^{i2}_{n(p)}}{\Delta V^{i2}_{n(n)}}\right)}{\left(1 - \frac{\Delta V^{i1}_{p(n)}}{\Delta V^{i1}_{p(p)}} \frac{\Delta V^{i2}_{n(p)}}{\Delta V^{i2}_{n(n)}}\right)} \\ I^{i1}_{p0} &= I^{i1}_{p(0)} - Y^i_{pp} V^{i1}_{p(0)} - Y^i_{pn} V^{i2}_{n(0)} \\ I^{i2}_{n0} &= I^{i2}_{n(0)} - Y^i_{np} V^{i1}_{p(0)} - Y^i_{nn} V^{i2}_{n(0)} \end{aligned} \tag{6}$$

Where $\Delta V^{i1}_{p(p)}$, $\Delta V^{i2}_{n(n)}$, $\Delta V^{i1}_{p(p)}$, and $\Delta V^{i2}_{n(n)}$ refer to the changes caused by positive and negative sequence single-tone voltage perturbations respectively. In addition, $\Delta V^{i1}_{p(n)}$, $\Delta V^{i2}_{n(p)}$, $\Delta I^{i1}_{p(n)}$, and $\Delta I^{i2}_{n(p)}$ represent the sequence coupling effects on the opposite sequence voltages and currents. Note that i1-index refers to the positive sequence perturbations at frequency of "$f_i + f_0$", and i2-index implies the negative sequence perturbations at frequency of "$f_i - f_0$" respectively.

Further approximation have been used by neglecting the effect of the sequence couplings in voltage (i.e. $\Delta V^{i1}_{p(n)} \approx 0$, $\Delta V^{i2}_{n(p)} \approx 0$) and simplifying Equation (6) to Equation (7) [8–10, 19–21, 30]:

$$\begin{aligned} Y^i_{pp} &= \frac{\Delta I^{i1}_{p(p)}}{\Delta V^{i1}_{p(p)}}, \quad Y^i_{pn} = \frac{\Delta I^{i1}_{p(n)}}{\Delta V^{i2}_{n(n)}} \\ Y^i_{nn} &= \frac{\Delta I^{i2}_{n(n)}}{\Delta V^{i2}_{n(n)}}, \quad Y^i_{np} = \frac{\Delta I^{i2}_{n(p)}}{\Delta V^{i1}_{p(p)}} \end{aligned} \tag{7}$$

This way, the admittance matrices indicate the DUT response's sensitivity to the presence of harmonic voltages at the terminal of the DUT. Note that the sensitivity level depends on the DUT's electrical components and control system [19–21, 26].

2.6 | Thevenin impedance derivation

It is important to note that using voltage perturbation tests; the impedances should be derived from the admittance matrices. In this way, let's consider that the Norton equivalent in Equation (1) has a dual Thevenin equivalent as Equation (8)[14]:

$$\begin{aligned} V_p^{i1} &= Z_{pp}^i I_p^{i1} + Z_{pn}^i I_n^{i2} + V_{p0}^{i1} \\ V_n^{i2} &= Z_{np}^i I_p^{i1} + Z_{nn}^i I_n^{i2} + V_{n0}^{i2} \end{aligned} \tag{8}$$

Hence, the impedance can be derived from the admittance matrices as follows:

$$\begin{aligned} Z_{pp}^i &= \frac{Y_{nn}^i}{Y_{pp}^i Y_{nn}^i - Y_{pn}^i Y_{np}^i} \\ Z_{pn}^i &= \frac{-Y_{pn}^i}{Y_{pp}^i Y_{nn}^i - Y_{pn}^i Y_{np}^i} \\ Z_{nn}^i &= \frac{Y_{pp}^i}{Y_{pp}^i Y_{nn}^i - Y_{pn}^i Y_{np}^i} \\ Z_{np}^i &= \frac{-Y_{np}^i}{Y_{pp}^i Y_{nn}^i - Y_{pn}^i Y_{np}^i} \end{aligned} \tag{9}$$

Furthermore, by neglecting the sequence couplings in current components (i. g. $\Delta I_{p(n)}^{i1} \approx 0, \Delta I_{n(p)}^{i2} \approx 0$), the impedances would be calculated directly from the voltage perturbations as follows:

$$\begin{aligned} Z_{pp}^i &= \frac{1}{Y_{pp}^i} = \frac{\Delta V_{p(p)}^{i1}}{\Delta I_{p(p)}^{i1}}, \quad Z_{pn}^i \approx 0 \\ Z_{nn}^i &= \frac{1}{Y_{nn}^i} = \frac{\Delta V_{n(n)}^{i2}}{\Delta I_{n(n)}^{i2}}, \quad Z_{np}^i \approx 0 \end{aligned} \tag{10}$$

However, omitting the current sequence couplings could add considerable inaccuracy to the test results, especially in the case of unbalanced systems [26]. This fact has been ignored in the previous impedance measurement procedures [8–10, 19–22], and [30].

As another option, the Thevenin impedance can be calculated using current perturbation tests via an additional shunt current source device in the test bench [18–25]. The impedance calculation procedure for current perturbation tests is given in the Appendix A of this paper.

2.7 | Model validation or empirical modelling applications

After finalising the perturbation tests for the chosen frequency range and the model calculation procedure, the results can be compared with the vendor models or simulation models. This way, the accuracy of the simulation models can be evaluated and corrections can be applied [9].

Another application of the test results can be extracting the empirical models. The empirical modelling refers to the model calculation of black-box systems only based on the tests and measurements. Therefore, it is assumed that there is no specific information about the system (e.g. control or simulation model) [9–11, 34]. In such cases, the aim of the tests is to derive the multi-frequency model of the converter system for a reasonable step-size (i.e. resolution) and frequency range [34]. The converter model would be estimated for the frequencies between the test steps to gain a higher resolution model.

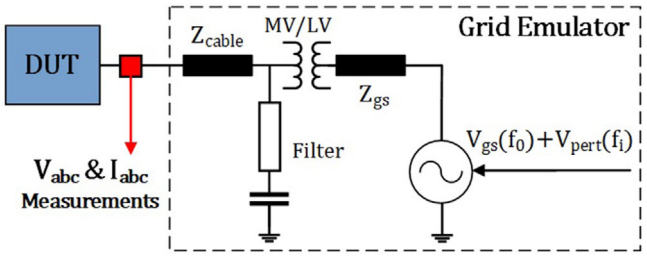

FIGURE 3 Example of voltage perturbation structure by a grid emulator

TABLE 1 Proposed specifications for small-signal perturbation tests

Specification	$f_h < f_0$	$f_0 \leq f_h < 2f_0$	$2f_0 \leq f_h < f_{h(\max)}$
V_h range	0.4%–0.6%	0.8%–1.2%	1.5%–2.5%
I_h range	5%–8%	3%–5%	1%–3%
Min. frequency	9Hz	f_0+1	$2f_0$
Max. f step	2Hz	2Hz	2Hz
Power ref. (pu)	0.1, 0.5, 1.0	0.1, 0.5, 1.0	0.1, 0.5, 1.0
Test period (s)	3–11	3–11	3–11

3 | TECHNICAL RECOMMENDATIONS FOR TRUSTWORTHY TEST RESULTS

Example structure of voltage perturbation tests using a grid emulator is illustrated in Figure 3. Accordingly, the perturbation voltage is added to the control reference signal of the grid emulator converter to be emulated at the terminal of the DUT [29–31]. In this part, the impacts of a grid emulator, DUT, and measurement equipment on the test results are explained. Accordingly, the perturbation test specifications are proposed in Table 1. Note that the quantified specifications are verified by the experimental test results demonstrated in Part IV.

3.1 | Impacts of the grid emulator on the test results

3.1.1 | Control system of the grid emulator

In the test structure shown in Figure 3, the grid emulator can be counted as a controlled voltage source interconnected with

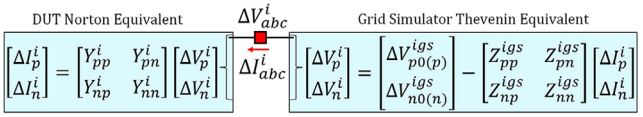

FIGURE 4 Small-signal equivalence of the interconnection between the DUT and the grid emulator

the DUT converter. The equivalent small-signal representation of the interconnection between the DUT and the grid emulator is illustrated in Figure 4. Accordingly, the grid emulator is represented by a Thevenin model, and a Norton equivalence depicts the DUT at the frequency of f_i. Note that Z_{pp}^{igs} and Z_{nn}^{igs} are positive and negative sequence impedances, respectively. Z_{pn}^{igs} and Z_{np}^{igs} refer to the couplings between the sequences. In addition, $\Delta V_{p0(p)}^{igs}$ and $\Delta V_{n0(n)}^{gs}$ depict the equivalent perturbation amplitudes. Note that $\Delta V_{p0(p)}^{igs}$ is only non-zero during the positive sequence perturbation and $\Delta V_{n0(n)}^{igs}$ is non-zero only during the negative sequence perturbations.

As shown in Figure 4, the grid emulator's non-linear control or hardware system can impose interactions and uncertainties on the test results rather than an ideal voltage source. This issue can be extended for any test device designed for perturbations. Effects of the grid emulator impedance on perturbation test results have been investigated in [19, 30]. Accordingly, the coupling impedances in the grid emulator ($Z_{pn}^{igs} \neq 0$ and $Z_{np}^{igs} \neq 0$) would lead to different and inappropriate results for voltage and current perturbation tests [19]. The frequency couplings can exist due to non-linear control, and sequence couplings can be generated by asymmetries in a three-phase system [26, 34]. Therefore, the grid emulator should have a linear control and symmetrical three-phase system to avoid different and doubtful results. A closed-loop control system can impose non-linearity and couplings in converters of a grid emulator. Therefore, this paper recommends adjusting open-loop voltage set-points for perturbations, as shown in Figure 3. In this way, the coupling impedances and unwanted control interactions can be eliminated. Typically, grid emulators' short circuit ratio is relatively higher than DUTs [27–30]; hence, linear and low amplitude impedance for the grid emulator can be realised using open-loop references for the voltage (V_{pert} and V_{gs}). Note that the feed-backs for the protection measures in the test bench should remain activated.

3.1.2 | Effect of grid emulator's output filter

The output filter of a grid emulator is required to limit its total harmonic distortion (THD) within an acceptable range [27–30] and [36]. However, the output filter can affect the voltage perturbation tests as well [30]. Assuming an open-loop control for a grid emulator, Z_{pp}^{igs} and Z_{nn}^{igs} can be regarded as an RLC filter impedance with cut-off frequency of f_{coff}^{gs}. Figure 5 illustrates an example of an RLC filter impedance seen from its output

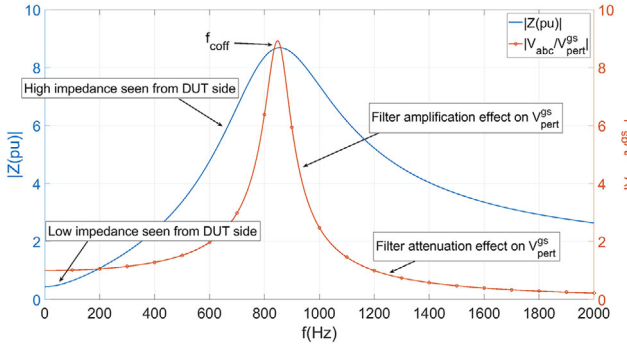

FIGURE 5 Example of effects of a grid emulator's RLC filter on perturbation tests: Filter impedance seen from DUT side (Z(pu)), and voltage gain on the perturbation voltage ($V_{abc}/V_{\text{pert}}^{gs}$)

terminal ($|Z(pu)|$). This impedance depicts an example of a grid emulator's impedance seen from the DUT side during perturbation tests. Accordingly, the DUT is exposed to a frequency-dependent impedance with low amplitudes in low frequency range and high amplitudes in high frequency range. Therefore, high current flow is expected for low frequency range which should be taken into account in the perturbation test specifications. Furthermore, very high impedance can lead to very low current responses as such to be out of the measurement resolution. For an accurate impedance calculation, the amplitude of the current response should be in a measurable range. Therefore, the amplitude of the perturbations should be adjusted over the testing frequency range.

Besides, an example of the filter effects on its input voltage or the perturbation voltage ($|V^{abc}/V_{\text{pert}}^{gs}|$) is shown in Figure 5. According to the voltage gain plot, the output filter of a grid emulator attenuates or eliminates the voltage perturbations with frequencies higher than the cut-off frequency (i.e. f_{coff}^{gs}). This fact limits the application of the grid emulator to the frequencies less than f_{coff}^{gs}. Furthermore, there could be voltage amplification effects in the frequencies around f_{coff}^{gs} [30]. In [30] it is recommended to measure the grid emulator's impedance before connecting to the DUT and modify the perturbation amplitudes accordingly.

It should be noted that the main interactions and non-linear impedance of a renewable energy generator (REG) occur in the range of its control bandwidth [11]. Typically, the control bandwidth of REGs is designed in the range of ($f_{bw}^{\text{dut}} < f_{sw}^{\text{dut}}/5$) [6–11]. Therefore, the perturbation frequency limitation of a grid emulator can be neglected as long as it is able to inject up to $f_{h(\max)}$ ($f_{bw}^{\text{dut}} < f_{h(\max)} < f_{sw}^{\text{dut}}/2$). Besides, re-tuning the grid emulator's filter configuration (f_{coff}^{gs}) can be a solution for perturbations in high frequencies.

3.1.3 | Background harmonic emissions from grid emulator

Harmonic emissions from a grid emulator's converters can cause an additional error in the test results [30]. Hence, it is

essential to include the initial emissions (or the initial condition without perturbation) in calculations, as suggested in Equations (4–6). In [37], a method is proposed to determine and separate the emissions of the grid emulators for the extreme conditions.

3.2 | Impacts of the DUT system

3.2.1 | Response current and voltage amplitudes

A perturbation may inevitably excite a resonance frequency or near resonance frequency of a DUT system. In such cases, the excessive voltage or current could present in the DUT response [29, 30, 32]. On the other hand, the parallel impedance branch of transformers and impedance of inductive components have small amplitudes in low frequencies. Thus, the voltage perturbation tests in very low frequencies would lead to high amplitudes of current responses. The amplitude of the perturbation voltage should be kept in a standard permissible range. Similarly, high amplitudes of voltage responses would be expected for current perturbation tests in high frequencies. As a suggestion, maximum permitted harmonic amplitudes and total harmonic distortion (THD) levels for AC grids can be derived from IEC 61000-3-6 [35]. Accordingly, the maximum levels are dependent on the system voltage level and the frequency of harmonics. The acceptable ranges for voltage or current perturbation are recommended in Table 1. Within the given ranges, lower values are recommended for high voltage test systems ($V_{abc} > 30$ kV).

3.2.2 | Protection measures in a DUT's control system

In a DUT control system, there could be potential protection measures for over-current, over-voltage, excessive THD, excessive reactive power, high RMS voltage value, and fault contingencies. Inappropriate perturbation tests can force the DUT control system into an abnormal protection scheme and lead to an inaccurate impedance measurement. Therefore, it is necessary to perform the tests within an acceptable range of amplitude and duration for perturbations, which are recommended in Table 1.

3.2.3 | Effective frequency range for perturbation

In general harmonic resonance issues would be considered up to the switching frequency of REGs (or f_{sw}^{dut}) [11]. Considering Nyquist's theorem in pulse-width modulation (PWM) techniques, the harmonics above half of a converter's switching frequency would not be constructed in its output. Therefore, a safe margin for the maximum frequency for perturbation tests is ($f_{h(\max)} < f_{sw}^{\mathrm{dut}}/2$). Furthermore, the electrical and digital filtering in converter systems eliminates the harmonics above the control bandwidth [6]-[11]. Therefore, the effective range of the control system interactions is mainly up to around the control bandwidth [6–11]. Thus, for higher frequencies, the effective part would be only the PWM emissions and electrical components, including transformer, converter switches, filters, and generator. In summary the maximum perturbation frequency would be chosen in the range of ($f_{bw}^{\mathrm{dut}} < f_{h(\max)} < f_{sw}^{\mathrm{dut}}/2$).

The minimum voltage perturbation frequency is limited due to the potentially high current responses, as mentioned in Part III.A-1. According to this fact, different perturbation ranges for sub-synchronous frequencies and minimum perturbation frequency are given in Table 1. Besides, since most interactions with phase-loop-locked (PLL) systems of converters occur in the range of less than $2f_0$ [6–11], smaller frequency steps and amplitudes are recommended for $f_h < 2f_0$. Moreover, in Table 1, addressing the frequency steps is intended to provide reasonable and practical resolutions for perturbation tests. According to the impedance models provided in the literature [5–11] and [17–21], sharp changes between 2 Hz steps are expected to be rare. However, after achieving overall impedance plots, specific resonance case studies would be performed locally with smaller steps such as 1 Hz around a potential resonance frequency. Smaller perturbation frequency steps would be used for deriving empirical models.

3.2.4 | DUT output power set-point

According to the state-of-the-art analytical models and validations in [5–10, 38, 39], the equivalent impedance of grid-connected converters and wind turbines are dependent on its output power (or current) references. This dependency can be evaluated by testing in different power set-points. Therefore, it is recommended to perform the perturbation tests at least for two different power set-points. In Table 1, three different power set-points are chosen to consider the effects of different operation points for REGs.

3.2.5 | Stable phase angle between voltage and current

A DUT's response against a perturbation may consist of dynamics over time, especially at the beginning of the injection due to delays in the DUT's control system response. Therefore, it is recommended to consider a short settling period and use the measurement data in the steady-state condition for admittance and impedance calculations. A stable phase angle between voltage and current harmonics is a sign of the steady-state condition. Furthermore, averaging of calculations from a perturbation period leads to more accurate results. In [14, 40], introduce prevailing angle ratio (PAR) as a practical criterion for evaluating dynamics in a harmonic emission that can be used to assess uncertainties in the DUT emission.

3.3 | Impacts of the measurement system

3.3.1 | Measurement equipment resolution

In IEC 61000-4-7 standard [33], it is recommended to utilise Class I measurement equipment for high precision applications. Accordingly, the frequency components of current or voltage to be measured would be in the range of "0.00002 pu up to 0.05 pu" [33]. Therefore, the accuracy of sensors and resolution of data acquisition modules should be chosen properly to cover a wide range of voltage and current amplitudes and frequencies. The minimum resolution ($RE_{\min(pu)}$) of the measurements in per-unit (pu) can be calculated as:

$$RE_{\min(pu)} = \left(\frac{X_{\max d(pu)}}{2^{N(\text{bits})}}\right)\left(\frac{X_{\max s}}{X_{\max t}}\right) \tag{11}$$

where $X_{\max d(pu)}$ refers to the maximum amplitude that is intended to be measured from a signal and N(bits) depicts the number of bits in the data acquisition modules. $X_{\max s}$ is the maximum analogue signal that a sensor can transfer to the data acquisition module and $X_{\max t}$ is the actual maximum analogue signal that the sensor is used to transmit. Note that $X_{\max s}$ is based on the sensor data-sheet, while $X_{\max t}$ is based on the actual application and equipment design. For instance, consider a data acquisition module with 18-bits resolution dedicated to measure up to 1.2 pu of a signal X, and an analogue sensor with maximum output of 0.2 V which is used to transmit maximum 0.18 V in response to the 1.2 pu of the signal X. According to 11, the minimum resolution would be $RE_{\min(pu)} = 5 \times 10^{-}6$ pu.

3.3.2 | Noise level consideration

Harmonic spectrum and DFT plots can illustrate the level of noise. In this way, the trustworthy data would be the values that are at least 20 times higher than the minimum resolution of measurement equipment (95% accuracy) [33]. For example, if the minimum resolution of measurement equipment was 5×10^{-6} pu, then the values higher than 100×10^{-6} pu could be used in the calculations with a high level of accuracy. According to IEC 61000-4-7 [33], Class I measurement equipment should have a maximum error of "±0.05% pu" for voltage measurements and "±0.15% pu" for current measurements in the small-signal range. Nowadays, more precise instruments have been used in the state-of-the-art test sites [29, 30].

4 | EXPERIMENTAL VERIFICATION OF THE PROPOSED TEST METHODOLOGY

The experimental single-tone voltage perturbation tests are performed by a 7 MVA grid emulator with 13.8 kV rated voltage at national renewable energy laboratory (NREL) Colorado, Golden, USA [9, 29]. The structure of the test bench is shown in Figure 3. The perturbation tests are performed on a 2 MVA PV converter and a 2 MVA Type 3 WT with three-phase balanced systems. Since, the structure of a Type 4 WT is similar to a PV converter, a general specification for converter-based renewable energy generators (REG) could be derived. The calculations are performed on instantaneous time-series measurement data from the terminal of WTs according to the proposed test methodology in Figure 2. The measurement equipment consists of 24-bits resolution and 50 k sample-per-second-per-channel (50 k S/s/channel) sample rate [29]. The frequency spectrum of the measured data is calculated by discrete Fourier transform (DFT) with 1 s frame window to achieve 1 Hz resolution according to IEC 61000-3-6 [35]. The perturbation tests are used for the verification of the proposed methodology by the following steps:

4.1 | Single-tone voltage perturbation tests to verify the proposed specifications

A group of single-tone perturbation tests is performed for the positive and negative sequences from 3 Hz up to 1 kHz. The tests are done for a 2 MVA PV converter and a 2 MVA Type 3 WT. The discrete Fourier transforms (DFT) of the experimental tests on the PV converter are given in Figure 6. Accordingly, Figure 6(a,b) illustrate the harmonic spectrum of normal operation condition without any perturbation ($V_{pv-p(0)}$ and $I_{pv-n(0)}$). Furthermore, Figure 5(c,d) illustrate the harmonic spectrum for positive sequence perturbations ($V_{pv-p(p)}$ and $I_{pv-n(p)}$). Note that the current response at each frequency is given for the same frequency of perturbation respectively and depicted by circle signs. Besides, the open-loop reference values (1% and 2%) are shown in the voltage spectrum. Accordingly, the emission effects around fundamental frequency are noteworthy, especially at 59 Hz with an amplitude of 5%. As mentioned in Part 3.2.3, this is mostly due to the grid emulator's initial emissions, which should be considered in the calculations. Moreover, in Figure 6(c), the attenuation effect of the grid emulator's output filter is visible for frequencies higher than 900 Hz, as explained in Part 3.2.2. Therefore, the grid emulator's efficient application with the existing filter structure would be in the range of less than 1 kHz. Besides, high current responses are observed in the sub-synchronous range (up to 0.085 pu for 9 Hz). Similarly, Figure 6(e,f) demonstrate the positive and negative sequence voltages and currents for negative sequence voltage perturbation ($V_{pv-p(n)}$ and $I_{pv-n(n)}$). Accordingly, the maximum current response has occurred in 5 Hz with an amplitude of 0.086 pu against 1% voltage perturbation.

Besides, the experimental voltage perturbation test results for a 2 MVA Type 3 wind turbine are demonstrated in Figure 7. Accordingly, the positive and negative voltage and current are illustrated for positive sequence perturbation tests ($V_{wt-p(p)}$ and $I_{wt-n(p)}$). The open-loop perturbation voltage references are given along with the measured values from the point of connection ($V_{p(\text{poc})}$) in Figure 7(a). Note that in this study case, the voltage perturbation at 59 Hz is applied in reverse with the grid emulator's emission. As a result, the voltage amplitude is maintained near a 1% value. Similar to Figure 6(c), the attenuation effect of the grid emulator's filter is observed in Figure 7(a)

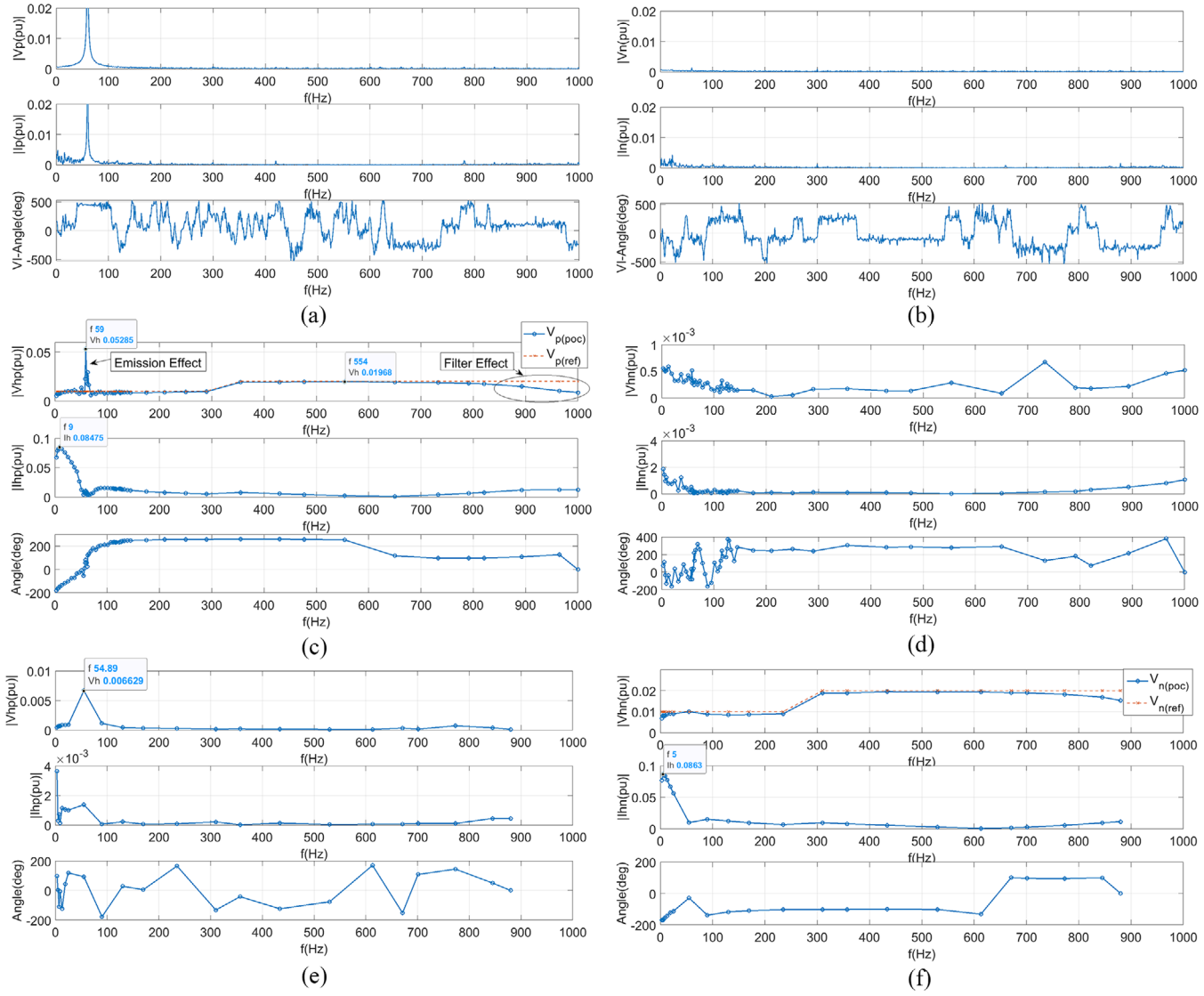

FIGURE 6 Positive and negative sequence voltages and currents for experimental single-tone voltage perturbations on a 2 MVA PV-converter: (a,b) Normal operation, (c,d) positive sequence perturbations, (e,f) negative sequence perturbations

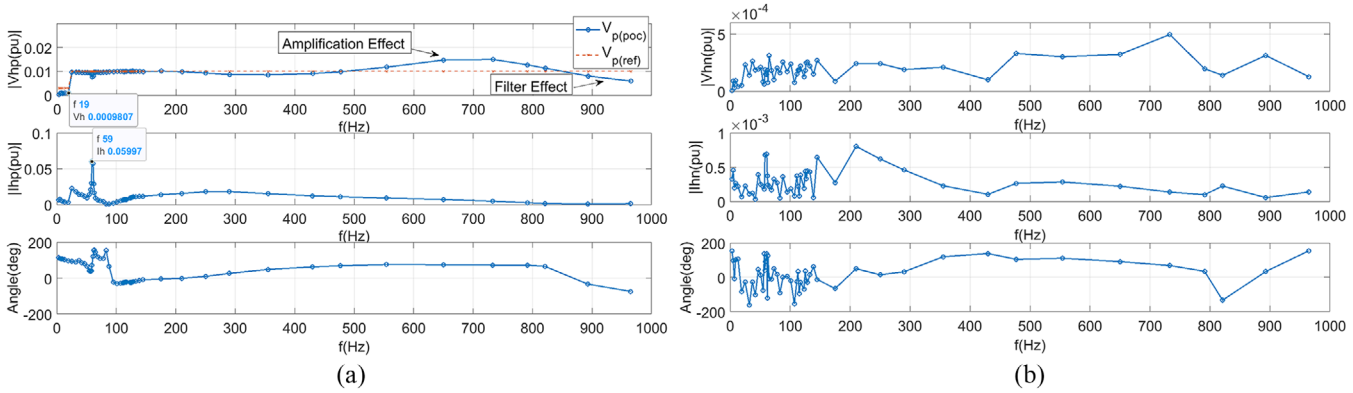

FIGURE 7 Positive and negative sequence voltages and currents for experimental positive sequence voltage perturbations on a 2 MVA Type 3 WT

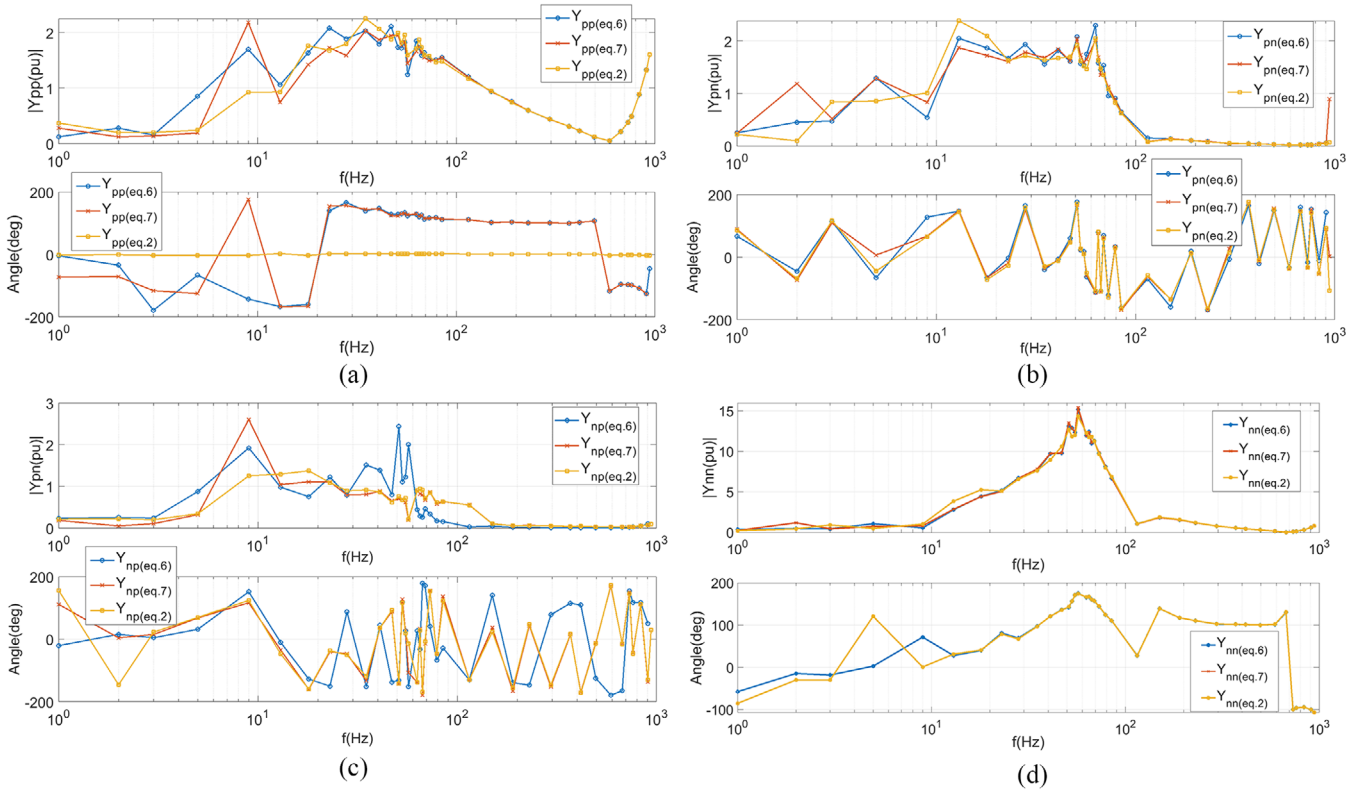

FIGURE 8 Comparison of admittance calculations for the 2 MVA PV converter with (Equation (6)) and without (Equations (2) and (7)) considering the sequence couplings, and with (Equations (6) and (7)) and without (Equation (2)) considering initial emissions

for frequencies higher than 900 Hz. It is noteworthy to mention that in the case of Type 3 WT, an amplification effect is observed in the range 500 to 800 Hz. This effect is caused by the WT mostly; since it has not been observed in the tests for the PV converter in Figure 6(c).

4.2 | Comparison of different simplifications in admittance and impedance calculation

The admittance matrices for the PV converter are calculated using Equation (6) and compared with the simplifications in Equations (2) and (7) in terms of couplings and initial emissions, as demonstrated in Figure 8. The amplitude and phase angle of admittance matrices are provided. A considerable difference has been observed in the range of less than 60 Hz for Y_{pv-pp} and Y_{pv-nn} plots. In addition, considerable errors are detected in coupling admittance (Y_{pv-pn} and Y_{pv-np}) in the range of less than 100 Hz. Thus, the couplings and initial emissions effects should be considered in the calculations using 6.

Furthermore, the derivation of the impedance matrices using different equations are illustrated in Figure 9. Accordingly, $Z_{pp(6,9)}$ stands for calculation of the impedance using Equations (6) and (9) without simplification. $Z_{pp(\text{eq.}7,9)}$ implies the calculations using Equations (7) and (9) with neglecting effects of coupled components in admittance calculations. In addition, $Z_{pp(\text{eq.}10)}$ implies the impedance calculations using Equation (10) with neglecting effects of coupled components in both admittance and impedance calculations. Thus, to achieve the most accurate impedance values, it is necessary to include the effects of the couplings in the calculations of admittance and impedance, even for a balanced system due to asymmetrical control.

5 | CONCLUSION

Despite the effectiveness of the impedance-based analysis for harmonic interaction studies, the necessity of a trustworthy test methodology for impedance model validation has been neglected in the literature. This paper proposed a general harmonic model validation test methodology for converter-based renewable energy generators using small-signal perturbation in the sequence domain. Furthermore, the technical specification (summarised in Table 1) and recommendations for trustworthy tests were provided. The technical recommendations include impacts of the device under test, grid emulator, and measurement equipment. The capability of the grid emulator in performing the perturbation tests is regarded as the main challenge.

The experimental verification of the test methodology is performed using a 7 MVA grid emulator on a 2 MVA PV converter and a 2 MVA Type 3 WT. The perturbation test specifications are derived from the MW-scale experiments. This way,

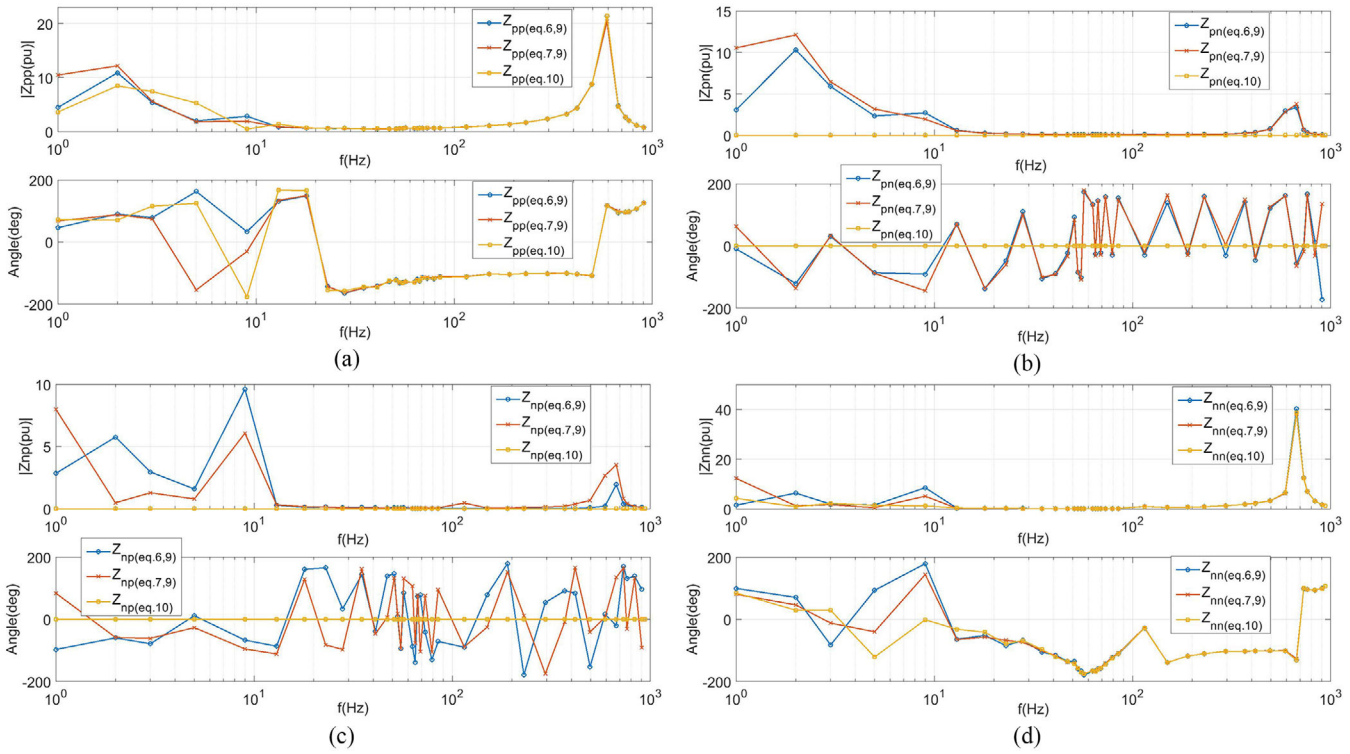

FIGURE 9 Comparison of impedance derivation for the 2MVA PV converter: Without simplification (Equations (6) and (9)); Neglecting the couplings in admittance (Equations (7) and (9)); Neglecting the couplings in admittance and impedance (Equation (10))

the application of a converter-based grid emulator for multi-frequency model validation purposes is verified and secured. Besides, the effects of simplifications in the model calculations, including effects of initial emissions and couplings, are investigated. Accordingly, the frequency and sequence couplings exist even in a balanced three-phase DUT system due to the asymmetrical control, especially in low-frequency ranges. Furthermore, the initial emissions may not be important in the harmonic stability studies but rather effective on the accurate calculation of the small-signal models. The evaluation of multi-tone perturbation tests and the assessment of the perturbation tests on networked converter systems are left out for future works.

ACKNOWLEDGEMENTS

This work was authored in part by Alliance for Sustainable Energy, LLC, the manager and operator of the National Renewable Energy Laboratory for the U.S. Department of Energy (DOE) under Contract No. DE-AC36-08GO28308. Funding provided by the U.S. Department of Energy Office of Energy Efficiency and Renewable Energy Wind Energy Technologies Office. The views expressed in the article do not necessarily represent the views of the DOE or the U.S. Government. The U.S. Government retains and the publisher, by accepting the article for publication, acknowledges that the U.S. Government retains a nonexclusive, paid-up, irrevocable, worldwide license to publish or reproduce the published form of this work or allow others to do so, for U.S. Government purposes.

ORCID

Behnam Nouri https://orcid.org/0000-0002-9188-7887
Łukasz Kocewiak https://orcid.org/0000-0002-9694-4027

REFERENCES

1. Kocewiak, Ł. H., Hjerrild, J., Bak, C.L.: Wind turbine converter control interaction with complex wind farm systems. IET Renewable Power Gener. 7(4), 380–389 (2013). https://ietresearch.onlinelibrary.wiley.com/doi/full/10.1049/iet-rpg.2012.0209
2. Kocewiak, Ł.H., et al.: Resonance damping in array cable systems by wind turbine active filtering in large offshore wind power plants. IET Renewable Power Gener. 11(7), 1069–1077 (2017). https://ietresearch.onlinelibrary.wiley.com/doi/full/10.1049/iet-rpg.2016.0111
3. Li, C.: Unstable operation of photovoltaic inverter from field experiences. IEEE Trans. Power Del. 33(2), 1013–1015 (2018)
4. Sun, J., et al.: A Theory for harmonics created by resonance in converter-Grid systems. IEEE Trans. Power Electron. 34(4), 3025–3029 (2019)
5. Kocewiak, Ł.H., et al.: Modelling of wind power plant transmission system for harmonic propagation and small-signal stability studies. IET Renewable Power Gener. 13(5), 717–724 (2019). https://ietresearch.onlinelibrary.wiley.com/doi/pdf/10.1049/iet-rpg.2018.5077
6. Cespedes, M., Sun, J.: Impedance modelling and analysis of grid-connected voltage-source converters. IEEE Trans. Power Electron. 29(3), 1254–1261 (2014)
7. Bakhshizadeh, M.K., et al.: Couplings in phase domain impedance modelling of grid-connected converters. IEEE Trans. Power Electron. 31(10), 6792–6796 (2016)
8. Shah, S., Parsa, L.: Impedance modelling of three-phase voltage source converters in DQ, Sequence, and phasor domains. IEEE Trans. Energy Convers. 32(3), 1139–1150 (2017)
9. Shah, S., et al.: Impedance methods for analyzing stability impacts of inverter-Based resources: Stability analysis tools for modern power

systems. IEEE Electrif. Mag. 9(1), 53–65 (2021). https://ieeexplore.ieee.org/document/9371238
10. Liao, Y., Wang, X.: Stationary-Frame complex-Valued frequency-Domain modelling of three-Phase power converters. in IEEE J. Emerging Selected Topics Power Electron. 8,2,1922–1933 (2020). doi: 10.1109/JESTPE.2019.2958938
11. Wang, X., Blaabjerg, F.: Harmonic stability in power electronic-Based power systems: Concept, modelling, and analysis. IEEE Trans. Smart Grid 10(3), 2858–2870 (2019)
12. IEEE Std 3002.8-2018: IEEE recommended practice for conducting Harmonic studies and analysis of industrial and commercial power systems, Technical Books Coordinating Committee of the IEEE Industry Applications Society Sep. (2018). https://mentor.ieee.org/3000-stds/dcn/19/stds-19-0004-00-PUBS-3002-8.pdf. Accessed August 2020
13. CIGRE TB 727: Modelling of inverter-Based generation for power system dynamic studies, Joint working group C4/C6.35/CIRED (May 2018). https://e-cigre.org/publication/727-modelling-of-inverter-based-generation-for-power-system-dynamic-studies
14. IEC TR 61400-21-3: 2019 – Wind energy generation systems – Part 21-3: Measurement and assessment of electrical characteristics – Wind turbine harmonic model and its application, International Electrotechnical Commission (Sep. 2019). https://webstore.iec.ch/publication/63755
15. CIGRE Study Committee C4, WG C4.49: Multi-frequency stability of converter-based modern power systems June (2018). http://digitalsubstation.com/wp-content/uploads/2018/06/TOR-WGC4.49_Multi-frequencystabilityofconverter-basedmodernpowersystems.pdf. Accessed December 2019
16. Kaveh, Malekian, et. al.: Harmonic model validation of power generation units. IET Renewable Power Gener. 14(13), 2456–2467 (2020)
17. Sun, J., Bing, Z., Karimi, K.J.: Input impedance modelling of multipulse rectifiers by harmonic linearization. IEEE Trans. Power Electron. 24(12), 2812–2820 (2009)
18. Huang, J., Corzine, K., Belkhayat, M.: Small-signal impedance measurement of power-electronics-based ac power systems using line-to-line current injection. IEEE Trans. Power Electron. 24(2), 445–455 (2009)
19. Rygg, A., et al.: A modified sequence-domain impedance definition and its equivalent to the dq-domain impedance definition for the stability analysis of ac power electronic systems. IEEE J. Emerg. Sel. Topics Power Electron. 4(4), 1383–1396 (2016)
20. Chauncey, G.L.: Impedance Measurement Techniques in Noisy Medium Voltage Power Hardware-in-the-Loop Environments (July 2018) http://purl.flvc.org/fsu/fd/2018_Su_Chauncey. Accessed October 2019
21. Gallo, D., et al.: A new test procedure to measure power electronic devices' frequency coupling admittance. IEEE Trans. Instrum. Meas. 67(10), 2401–2409 (2018)
22. Ruffing, P., et al.: Deliverable 16.3: Overview of the conducted tests, the results and the associated analyses with respect to the research questions and analyses within WP3. PROMOTion - Progress on Meshed HVDC Offshore Transmission Networks, Feb. 2020. https://www.promotion-offshore.net/fileadmin/PDFs/D16.3_Overview_of_the_conducted_tests_the_results_and_the_associated_analyses_with_respect_to_the_research_questions_and_analyses_within_WP3.pdf. Accessed on March 2020
23. Wilken, H., Jordan, M., Schulz, D.: Spectral grid impedance identification on the low-, medium- and high-voltage level – system design, realization and measurement results of grid impedance measurement devices. Advances Sci., Technol. Eng. Syst. J. 4(1), 8–16 (2019)
24. Salis, V., et al.: Experimental validation of harmonic impedance measurement and LTP nyquist criterion for stability analysis in power converter networks. IEEE Trans. Power Electron. 34(8), 7972–7982 (2019)
25. Luhtala, et al.: Identification of three-phase grid impedance in the presence of parallel converters. Energies 12(14), 2674 (2019)
26. Zong, H., et al.: Block diagonal dominance-based model reduction method applied to MMC asymmetric stability analysis. IEEE Trans. Energy Conversion (2021). doi: 10.1109/TEC.2021.3054925
27. Nouri, B., et al.: Generic characterization of electrical test benches for AC- and HVDC-connected wind power plants. Wind Ener. Sci. 5, 561–575 (2020). https://wes.copernicus.org/articles/5/561/2020/
28. Jassmann, U., et al.: CertBench: Conclusions from the comparison of certification results derived on system test benches and in the field. Forsch Ingenieurwes 85, 353–371 (2021)
29. Shah, S., et al.: Impedance measurement of wind turbines using a multi-megawatt grid emulator. Paper presented at 18th Wind Integration Workshop, Dublin, 16–18 Oct 2019
30. Azarian, S., et al.: Experimental impedance measurement of SG DD-167 Variable-Speed Direct-Drive Wind Turbine by power electronic grid emulator of Fraunhofer IWES DyNaLab. Paper presented at 19th Wind Integration Workshop, Energynautics, Berlin, 11–12 Nov 2020
31. Quester, M., et al.: Online impedance measurement of a modular multilevel converter. In: 2019 IEEE PES Innovative Smart Grid Technol. Europe (ISGT-Europe), pp. 1–5. IEEE, Piscataway, NJ (2019)
32. Nouri, B., Kocewiak, Ł., Sørensen, P.: Frequency and sequence couplings in type 4 and Type 3 wind turbines. Paper presented at 19th Wind Integr. Workshop, Energynautics, Berlin, 11–12 Nov. 2020
33. Electromagnetic compatibility (EMC) 61000– Part 4–7. Testing and measurement techniques–General guide on harmonics and interharmonics measurements and instrumentation, for power supply systems and equipment connected thereto. International Electro-technical Commission. https://webstore.iec.ch/publication/4228. Accessed October 2009
34. Bakhshizadeh, M.K., et al.: A numerical matrix-based method for stability and power quality studies based on harmonic transfer functions. IEEE J. Emerging Selected Topics Power Electron. 5(4), 1542–1552 (2017)
35. Electromagnetic compatibility (EMC) 61000-Part 3–6. Limits-Assessment of emission limits for the connection of distorting installations to MV, HV and EHV power systems. International Electro-technical Commission. https://webstore.iec.ch/publication/4155. Accessed Feb. 2008
36. Beres, R. N., et al.: A review of passive power filters for three-phase grid-connected voltage-source converters. IEEE J. Emerging Selected Topics Power Electron. 4(1), 54–69 (2016)
37. ABB Schweiz AG.: A procedure for the impedance calculation of grid emulators. European Patent EP3,828,557, June 2021
38. Vieto, I., Sun, J.: Refined small-signal sequence impedance models of type-III wind turbine. In: IEEE Energy Convers. Congress Exposition (ECCE), pp. 2242–2249. IEEE, Piscataway, NJ (2018)
39. Yang-Wu, S., et al.: Harmonic modelling and experimental validation of the converters of DFIG-based wind generation system. Complexity 2019, 7968914 (2019)
40. Christensen, L.S., Nielsen, J.G., Lund, T.: Using prevailing angle of harmonics to distinguish between background noise and emission from a turbine. Paper presented at 16th Wind Integration Workshop, Energynautics, Berlin, 25–27 Oct 2017

How to cite this article: Nouri, B., et al.: Test methodology for validation of multi-frequency models of renewable energy generators using small-signal perturbations. IET Renew. Power Gener. 15, 3564–3576 (2021). https://doi.org/10.1049/rpg2.12245

APPENDIX A: IMPEDANCE CALCULATION BASED ON CURRENT PERTURBATION TESTS

The Thevenin equivalent can be calculated based on Equation (8) and using three different measurement data, including without perturbation, positive and negative sequence current

perturbations as follows:

$$
\begin{aligned}
Z^{i}_{pp} &= \frac{\Delta V^{i1}_{p(p)}}{\Delta I^{i1}_{p(p)}} \frac{(1-\frac{\Delta V^{i1}_{p(n)}}{\Delta V^{i1}_{p(p)}}\frac{\Delta I^{i2}_{n(p)}}{\Delta I^{i2}_{n(n)}})}{(1-\frac{\Delta I^{i1}_{p(n)}}{\Delta I^{i1}_{p(p)}}\frac{\Delta I^{i2}_{n(p)}}{\Delta I^{i2}_{n(n)}})} \\
Z^{i}_{pn} &= \frac{\Delta V^{i1}_{p(n)}}{\Delta I^{i2}_{n(n)}} \frac{(1-\frac{\Delta V^{i1}_{p(p)}}{\Delta V^{i1}_{p(n)}}\frac{\Delta I^{i1}_{p(n)}}{\Delta I^{i1}_{p(p)}})}{(1-\frac{\Delta I^{i1}_{p(n)}}{\Delta I^{i1}_{p(p)}}\frac{\Delta I^{i2}_{n(p)}}{\Delta I^{i2}_{n(n)}})} \\
Z^{i}_{nn} &= \frac{\Delta V^{i2}_{n(n)}}{\Delta I^{i2}_{n(n)}} \frac{(1-\frac{\Delta V^{i2}_{n(p)}}{\Delta V^{i2}_{n(n)}}\frac{\Delta I^{i1}_{p(n)}}{\Delta I^{i1}_{p(p)}})}{(1-\frac{\Delta I^{i1}_{p(n)}}{\Delta I^{i1}_{p(p)}}\frac{\Delta I^{i2}_{n(p)}}{\Delta I^{i2}_{n(n)}})} \\
Z^{i}_{np} &= \frac{\Delta V^{i2}_{n(p)}}{\Delta I^{i1}_{p(p)}} \frac{(1-\frac{\Delta V^{i2}_{n(n)}}{\Delta V^{i2}_{n(p)}}\frac{\Delta V^{i2}_{n(p)}}{\Delta V^{i2}_{n(n)}})}{(1-\frac{\Delta I^{i1}_{p(n)}}{\Delta I^{i1}_{p(p)}}\frac{\Delta I^{i2}_{n(p)}}{\Delta I^{i2}_{n(n)}})}
\end{aligned}
\tag{A.1}
$$

$$
\begin{aligned}
V^{i1}_{p0} &= V^{i1}_{p(0)} - Z^{i}_{pp} I^{i1}_{p(0)} - Z^{i}_{pn} I^{i2}_{n(0)} \\
V^{i2}_{n0} &= V^{i2}_{n(0)} - Z^{i}_{np} I^{i1}_{p(0)} - Z^{i}_{nn} I^{i2}_{n(0)}
\end{aligned}
$$

Note that i1-index refers to the positive sequence current perturbations at frequency of "$f_i + f_0$", and i2-index implies the negative sequence current perturbations at frequency of "$f_i - f_0$" respectively. Δ sign refers to the changes caused by positive and negative sequence single-tone current perturbations. $I^{i1}_{p(p)}$ and $I^{i2}_{n(n)}$ refer to positive and negative sequence single-tone current injections respectively. The Equation (A.1) can be simplified by neglecting the effects of voltage responses on currents in coupled frequencies (i. g. $\Delta I^{i1}_{p(n)} \approx 0$, $\Delta I^{i2}_{n(p)} \approx 0$) as follows:

$$
\begin{aligned}
Z^{i}_{pp} &= \frac{\Delta V^{i1}_{p(p)}}{\Delta I^{i1}_{p(p)}}, Z^{i}_{pn} = \frac{\Delta V^{i1}_{p(n)}}{\Delta I^{i2}_{n(n)}} \\
Z^{i}_{nn} &= \frac{\Delta V^{i2}_{n(n)}}{\Delta I^{i2}_{n(n)}}, Z^{i}_{np} = \frac{\Delta V^{i2}_{n(p)}}{\Delta I^{i1}_{p(p)}}
\end{aligned}
\tag{A.2}
$$